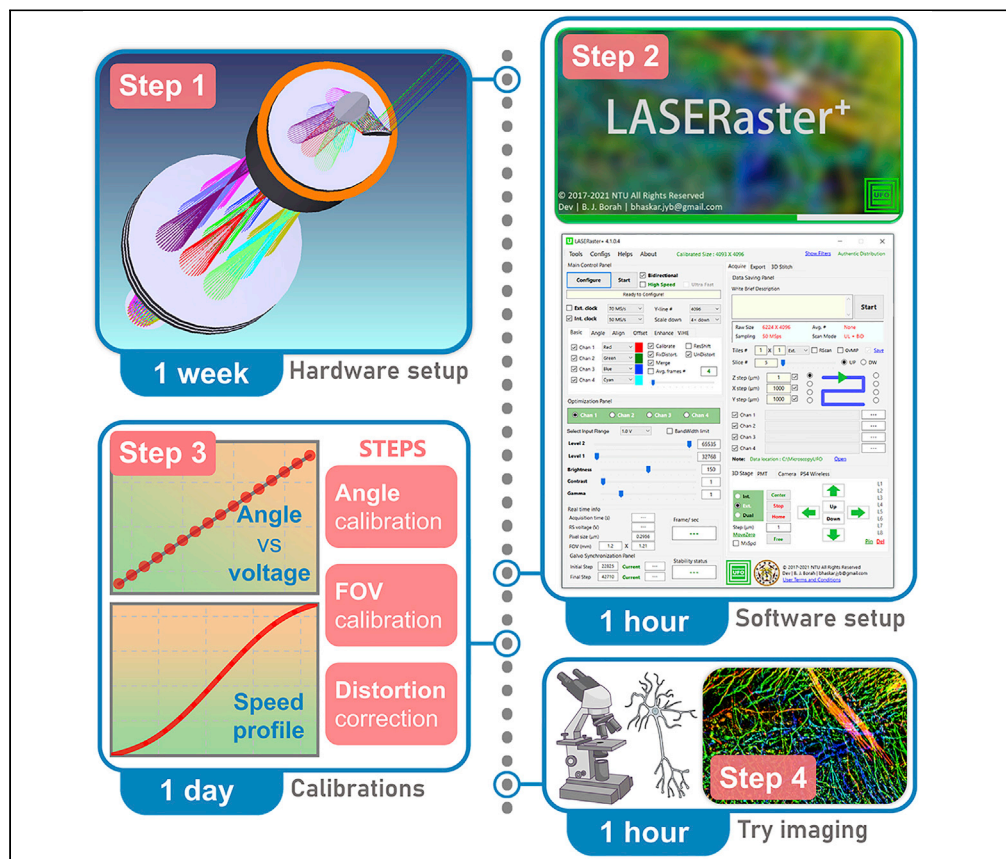


Protocol

Construction of a high-NFOM multiphoton microscope with large-angle resonant raster scanning



A resonant-scanning multiphoton optical microscope (MPM) with a millimeter-scale field-of-view (FOV) often encounters a poor Nyquist figure-of-merit (NFOM), leading to an aliasing effect owing to limited effective voxel-sampling rate. In this protocol, we provide a design guideline to enable high-NFOM MPM imaging while simultaneously securing a large FOV/digital-resolution ratio and a fast resonant raster-scanning speed. We further provide a free version of our custom acquisition software to assist with a smooth and easy construction process.

Bhaskar Jyoti Borah,
Chi-Kuang Sun

bhaskar.jyb@gmail.com
(B.J.B.)
sun@ntu.edu.tw (C.-K.S.)

Highlights

Critical guidelines to build a high-NFOM laser-scanning multiphoton optical microscope

An optimized optical design for large-angle resonant-galvo raster scanning

A simplified electronic design for high-speed raster scanning

A free-version of C++ based control and acquisition software (LASERaster⁺)

Borah & Sun, STAR Protocols
3, 101330
June 17, 2022 © 2022 The
Authors.
<https://doi.org/10.1016/j.xpro.2022.101330>



Protocol

Construction of a high-NFOM multiphoton microscope with large-angle resonant raster scanning

Bhaskar Jyoti Borah^{1,4,*} and Chi-Kuang Sun^{1,2,3,5,*}¹Department of Electrical Engineering and Graduate Institute of Photonics and Optoelectronics, National Taiwan University, Taipei 10617, Taiwan²Graduate Institute of Biomedical Electronics and Bioinformatics, National Taiwan University, Taipei 10617, Taiwan³Molecular Imaging Center, National Taiwan University, Taipei 10617, Taiwan⁴Technical contact⁵Lead contact*Correspondence: bhaskar.jyb@gmail.com (B.J.B.), sun@ntu.edu.tw (C.-K.S.)
<https://doi.org/10.1016/j.xpro.2022.101330>

SUMMARY

A resonant-scanning multiphoton optical microscope (MPM) with a millimeter-scale field-of-view (FOV) often encounters a poor Nyquist figure-of-merit (NFOM), leading to an aliasing effect owing to limited effective voxel-sampling rate. In this protocol, we provide a design guideline to enable high-NFOM MPM imaging while simultaneously securing a large FOV/digital-resolution ratio and a fast resonant raster-scanning speed. We further provide a free version of our custom acquisition software to assist with a smooth and easy construction process.

For complete details on the use and execution of this protocol, please refer to Borah et al. (2021).

BEFORE YOU BEGIN

The background

Owing to a near-infrared (NIR) excitation spectrum, a laser-scanning multiphoton optical microscope (MPM) or a multimodal nonlinear optical microscope (NLOM) (Denk et al., 1990; Yue et al., 2011; Li et al., 2018; Zipfel et al., 2003) becomes superior to single-photon-based imaging modalities in the context of millimeter-scale penetration capability. However, the NLOM's FOV with a high numerical aperture (NA) objective lens is limited to a sub-millimeter regime (Zhang et al., 2019) and thus might require extensive digital image stitching or mosaicking operations especially while targeting a centimeter-scale imaging area. Therefore, a large enough FOV is always being a necessity to minimize stitching operations and thus to facilitate a faster imaging speed. It is important to note that a moderate or low magnification objective lens can help extend an FOV up to several millimeters, while its moderate NA can simultaneously preserve an adequate optical resolution (Tsai et al., 2015; Bumstead et al., 2018; Terada et al., 2018; Stirman et al., 2016; Sofroniew et al., 2016). However, to take advantage of such large FOV and high optical resolution simultaneously without a need for optical zooming, we must be able to properly digitize the signal with adequate sampling frequency.

In the context of any digital systems involving digitization of an analog signal, the Nyquist-Shannon criterion (Nyquist, 1928; Shannon, 1949) enforces the sampling frequency to be at least twice the maximum frequency of the analog signal to avoid the phenomenon of *aliasing*. In a digital microscopy/imaging system, undersampling-induced *aliasing* might convert the optics-limited high spatial frequencies of the objects into low spatial frequencies in the final image by the Moiré effect (Pawley, 2006; Heintzmann and Sheppard, 2007). An adequate digitization capability thus becomes an imperative factor to digitally retrieve a submicron optical resolution over a large millimeter-scale



FOV. It is noteworthy that maintaining a high spatial sampling frequency is fairly straightforward if we are not concerning an imaging speed. For instance, a slow galvanometric scanner can be easily implemented instead of a fast resonant scanner (along the fast axis), which will however drastically limit the effective scanning area per unit second. On the other hand, to ensure a fast kilohertz raster-scanning and simultaneously a submicron digital resolution, a high enough effective voxel-sampling rate, or image-pixel sampling rate, would be necessary to ensure an adequate number of pixels on each fast-axis line, and thereby to satisfy or even exceed the respective Nyquist-Shannon criterion. While discussing a voxel-sampling rate, we also need to consider the digitization strategy in an MPM. Owing to a typically used pulsed-laser source, the maximum effective voxel-sampling rate gets restricted by the repetition rate of the laser itself, with the fact that each digitized voxel is expected to correspond to at least one optical pulse. In other words, simply opting for a high sampling rate digitization cannot solve the issue of *aliasing*. A high repetition-rate laser in an MPM is indeed crucial to enable a high voxel-sampling rate.

The protocol

This protocol illustrates a step-by-step guideline to construct a kilohertz resonant-scanning MPM with a large FOV/digital-resolution ratio of more than 3000, while simultaneously securing a high (≥ 1) Nyquist figure-of-merit (Borah et al., 2021). This protocol is useful if you wish not to compromise with raster-scanning speed yet target an optical-zoom-free submicron digital resolution across a millimeter-scale FOV. In this protocol, you would first comprehend a few important mathematical expressions relating an MPM FOV to a laser-repetition rate, which would help you select the best combination of a pulsed laser with your desired optomechanical specifications. You would then construct a large-angle optical raster scanning (LAORS) system and its associated fluorescence detection unit, and subsequently, a control and data acquisition system to enable a high-NFOM MPM imaging. You can obtain a free license of our custom software *LASERaster*⁺ developed and dedicated to operating with our specific opto-electro-mechanical designs.

△ CRITICAL: To follow the protocol, you are expected to be familiar with principles of nonlinear/multiphoton optical microscopy, pulsed lasers, optomechanical components, basic optical alignments, connecting/assembling electronic devices/components, and installing/operating computer software. Be sure to wear a certified laser safety glass with an adequate optical density when operating with a laser. Wear appropriate gloves while dealing with an uncovered electronic device to protect the same from electrostatic discharge.

KEY RESOURCES TABLE

REAGENT or RESOURCE	SOURCE	IDENTIFIER
Software and algorithms		
LASERaster ⁺ 4.1.0.4 (free license)	This report	https://ufo.ee.ntu.edu.tw/
AlazarTech C/C++ application program interface (API), 6.7.0 or newer	Alazar Technologies Inc., Canada	https://www.alazartech.com/
NI-DAQmx C API, 18.6.0 or newer	National Instruments Corporation, USA	https://www.ni.com/
CURL C/C++ API, 7.69.1 or newer	Open source	https://curl.se/
OpenCV (C++) 4.5.2, or newer	Open source	https://opencv.org/
Compute unified device architecture (CUDA) (11.4, update 2, or newer)	NVIDIA, USA	https://www.nvidia.com/
Optical components		
Objective lens (XLUMPlanFI, 20×/0.95W)	Olympus, Japan	https://www.olympus-global.com/
Scan lens (LSM05-BB), $f = 110$ mm	Thorlabs, USA	https://www.thorlabs.com/
General lens (86-925), $f = 500$ mm	Edmund Optics, USA	https://www.edmundoptics.com/
General lens (32-982), $f = 150$ mm	Edmund Optics, USA	https://www.edmundoptics.com/

(Continued on next page)

Continued		
REAGENT or RESOURCE	SOURCE	IDENTIFIER
General lens (48-654), $f = 40$ mm	Edmund Optics, USA	https://www.edmundoptics.com/
Dichroic beam-splitter (FF801-Di02 or FF735-Di02)	Semrock, USA	https://www.semrock.com/
Bandpass filter (e.g., FF01-580/60-25-D)	Semrock, USA	https://www.semrock.com/
Optional color filter (FGB37-A)	Thorlabs, USA	https://www.thorlabs.com/
Pulsed laser source		
Yb-fiber laser (Fidelity 2)	Coherent Inc., USA	https://www.coherent.com/
Raster-scanning system		
Resonant scanner (CRS 4 kHz)	Cambridge Technology, USA	https://www.cambridgetechnology.com/
Galvanometer scanner (8320K)	Cambridge Technology, USA	https://www.cambridgetechnology.com/
PCIe digitizer and interface I/O card & modules		
Digitizer (ATS9440)	Alazar Technologies Inc., Canada	https://www.alazartech.com/
Interface card (PCIe-6341)	National Instruments Corporation, USA	https://www.ni.com/
Digital to Analog Converter (DAC 6757)	Cambridge Technology, USA	https://www.cambridgetechnology.com/
Photomultiplier tube (PMT) and associated devices		
PMT (R10699)	Hamamatsu Photonics, Japan	https://www.hamamatsu.com/
Transimpedance amplifier (C6438-01)	Hamamatsu Photonics, Japan	https://www.hamamatsu.com/
High voltage supply (C9525)	Hamamatsu Photonics, Japan	https://www.hamamatsu.com/
Electronic stages & controller		
Linear stage (TSDM40-15X)	SIGMA KOKI, Japan	https://jp.optosigma.com/
Linear stage (SGSP80-20ZF)	SIGMA KOKI, Japan	https://jp.optosigma.com/
Controller (SHOT-304GS)	SIGMA KOKI, Japan	https://jp.optosigma.com/
Additional		
Voltage buffer (50LD)	Thorlabs, USA	https://www.thorlabs.com/
Power Splitter (ZFRSC-42-S+)	Mini-Circuits, USA	https://www.minicircuits.com/
Graphics card (Quadro RTX 8000)	NVIDIA, USA	https://www.nvidia.com/

MATERIALS AND EQUIPMENT

The custom software *LASERaster*⁺ was developed in Microsoft Visual Studio 2019 (Microsoft Corporation, USA). The GUI uses the .NET framework. All backend high-performance functions/codes are written in native C++. The software utilizes several application program interfaces (APIs): AlazarTech C/C++ API, NI-DAQmx C API, NVIDIA's compute unified device architecture (CUDA) (version: 11.4, update 2) accelerated C/C++ based OpenCV (an open-source computer vision library) (version: 4.5.2), CURL C++ API. Refer to the *ReadMe* directory after installation of *LASERaster*⁺ for more details. Note that *LASERaster*⁺ takes advantage of dual-port memory supported by AlazarTech digitizers allowing simultaneous data transfer to the host memory during ongoing data acquisition. CUDA-accelerated OpenCV algorithms allow high-speed data processing. *LASERaster*⁺ further implicates a multithreaded control algorithm for synchronization of slow Y-axis with fast X-axis without sending external electrical frame-trigger signal after completion of each frame. [Table 1](#) enlists the prerequisites for *LASERaster*⁺.

STEP-BY-STEP METHOD DETAILS

Theoretical considerations before you start

⌚ Timing: 30 min

1. The Nyquist-Shannon sampling theorem (Nyquist, 1928; Shannon, 1949) in the context of a digital microscopy/imaging system (Pawley, 2006; Heintzmann and Sheppard, 2007) demands the

Table 1. Dependency and prerequisites for the C++-based control and data acquisition software

Hardware requirements	
Computer	Motherboard chipset: X299, or newer Intel processor: minimum 6 cores, or 12 threads Single-core frequency: 3 GHz or more Minimum PCIe bus: one x16, one x8, one x4; each with full bandwidth (PCIe 3.0 standard)
Display resolution	Minimum: Full HD (1920 × 1080); recommended: 4k (3840 × 2160)
Graphics card	CUDA supported NVIDIA graphics card (used: Quadro RTX 8000)
Acquisition card	AlazarTech PCIe digitizer (used: ATS9440)
Interface card	National Instruments M-series or X-series multifunction I/O card with minimum of 24 digital I/O pins and at least one analog output pin (used: PCIe 6341)
Electronic 3D stage	Supported stages from Sigma Koki, Japan; recommended resolution of at least 1 μm (used controller: SHOT-304GS)
High voltage supply	Supported bench-top high voltage power supply from Hamamatsu Photonics, Japan; recommended: C9525
Software dependency	
	Operating system: Windows 10 (1809, or newer) Windows driver for NVIDIA CUDA supported graphics card; 30.0.0 or newer .NET framework 4.6.1, or newer NI-DAQmx Runtime (18.6 or newer) AlazarTech Windows driver for specific acquisition card (6.7.0 or newer) USB driver if necessary

size of each digitized pixel (d) to be at least half of the optics-limited resolution (r^{FWHM} , Zipfel et al., 2003; Sheppard and Gu, 1990), i.e.,

$$d \leq \frac{1}{2} r^{FWHM}, \quad (\text{Equation 1})$$

$$\text{where } r^{FWHM} = \begin{cases} \frac{0.532 \lambda_{exc}}{\sqrt{n} NA}, & NA \leq 0.7 \\ \frac{0.541 \lambda_{exc}}{\sqrt{n} NA^{0.91}}, & NA > 0.7 \end{cases}. \quad (\text{Equation 2})$$

λ_{exc} , n , and NA stand for excitation wavelength, order of the multiphoton process, and numerical aperture of the objective lens, respectively.

2. Following Equation (1), for a fast-axis field of view of FOV_{max} , the minimum required pixel number P_n can be given as

$$P_n = \frac{FOV_{max}}{d} = \frac{2 FOV_{max}}{r^{FWHM}}. \quad (\text{Equation 3})$$

3. For an f kHz resonant scanner, presuming a constant scan velocity and a bi-directional scanning with a $2f$ kHz line rate, the minimum effective voxel-sampling rate V_{min} to fulfill the Nyquist-Shannon criterion can be expressed as

$$V_{min} = \frac{4f FOV_{max}}{r^{FWHM}}. \quad (\text{Equation 4})$$

4. For an MPM utilizing a pulsed laser source, the required repetition rate (R) would thus be

$$R \geq V_{min} \times N, \quad (\text{Equation 5})$$

where N is an integer signifying number of optical pulse(s) per voxel, presuming a synchronized sampling to the laser optical pulses. Using Equation (2), for a general laser-scanning MPM, V_{min} can be represented as

$$V_{min} = \begin{cases} \frac{7.5188\sqrt{n} NA f \text{FOV}_{max}}{\lambda_{exc}}, & NA \leq 0.7 \\ \frac{7.3937\sqrt{n} NA^{0.91} f \text{FOV}_{max}}{\lambda_{exc}}, & NA > 0.7 \end{cases}. \quad (\text{Equation 6})$$

Considering $N = 1$ in Equation (5) for the optimized case, the minimum laser repetition rate required will be

$$R_{min} = V_{min}. \quad (\text{Equation 7})$$

5. To characterize a laser-scanning MPM in terms of its optical-resolution retrieving ability, a Nyquist figure-of-merit (NFOM) is formulated as

$$\text{NFOM} = \frac{V_{eff}}{V_{min}}, \quad (\text{Equation 8})$$

where V_{eff} is the effective voxel-sampling rate or the image-pixel sampling rate. In case of pulse-level synchronization, V_{eff} can be replaced with R/N , and thus substituting V_{eff} and V_{min} , Equation (8) can be written as

$$\text{NFOM} = \begin{cases} \frac{0.133 R \lambda_{exc}}{\sqrt{n} N f NA \text{FOV}_{max}}, & NA \leq 0.7 \\ \frac{0.1353 R \lambda_{exc}}{\sqrt{n} N f NA^{0.91} \text{FOV}_{max}}, & NA > 0.7 \end{cases}. \quad (\text{Equation 9})$$

6. Using Equation (9), for an optimized condition with $\text{NFOM} = 1$ and $N = 1$, the maximum achievable aliasing-free FOV for a specified set of laser, fast-axis scanner, and objective lens can be estimated as

$$\text{FOV}_{max} = \begin{cases} \frac{0.133 R \lambda_{exc}}{\sqrt{n} f NA}, & NA \leq 0.7 \\ \frac{0.1353 R \lambda_{exc}}{\sqrt{n} f NA^{0.91}}, & NA > 0.7 \end{cases}. \quad (\text{Equation 10})$$

For a conventional laser-scanning system (Chun et al., 2013), the optics-limited fast-axis field of view, FOV_{OL} can be determined as

$$\text{FOV}_{OL} = 2 \tan|\theta_{\pm}| \times \frac{f_o f_s}{f_t}, \quad (\text{Equation 11})$$

where θ_{\pm} is the fast-axis scan-angle by the scanning mirror with respect to the optical axis, f_o , f_s , and f_t are effective focal lengths of the objective lens, scan lens, and tube lens, respectively.

7. Following Equations (6), (7), and (11), and substituting FOV_{max} with FOV_{OL} , you can estimate the minimum required repetition rate as

$$R_{min} = \begin{cases} \frac{15.0376\sqrt{n} NA f \tan|\theta_{\pm}| f_o f_s}{\lambda_{exc} f_t}, & NA \leq 0.7 \\ \frac{14.7874\sqrt{n} NA^{0.91} f \tan|\theta_{\pm}| f_o f_s}{\lambda_{exc} f_t}, & NA > 0.7 \end{cases}. \quad (\text{Equation 12})$$

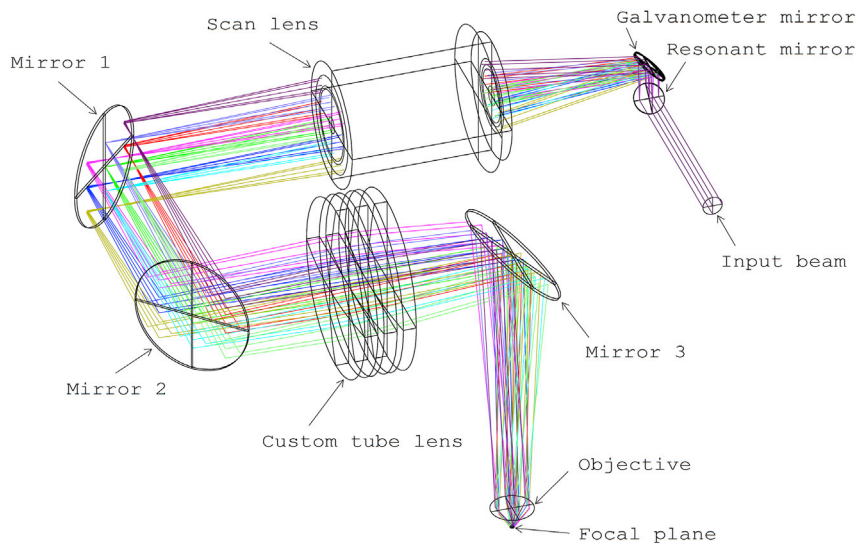


Figure 1. Schematics of LAORS system with Zemax ray tracing

Input beam: optical pulses from a pulsed laser source; resonant mirror: CRS 4 kHz (Cambridge Technology, USA); galvanometer mirror: 8320K (Cambridge Technology, USA); scan lens: LSM05-BB, effective focal length (EFL) of 110 mm (Thorlabs, USA); custom tube lens: a combination of 3 plano-convex lenses (Edmund Optics: 86-925, EFL of 500 mm), combined EFL of 166.7 mm; objective lens: Olympus XLUMPlanFI, 20 \times /0.95W. Note that multiple colors are utilized to better distinguish the rays under different scanning angles by the resonant and galvanometer scanning mirrors (see [Figure 2](#) for more information on optical performance at different scanning angles).

Construction of the large-angle optical raster scanning (LAORS) system

⌚ Timing: 1 day

8. Refer to [Figure 1](#) depicting the essential elements of a large-angle optical raster scanning (LAORS) system, primarily comprising:
 - a. a typical pulsed laser source with an adequate repetition rate (Fidelity 2, Coherent, USA),
 - b. a raster scanning unit with a resonant scanner (CRS 4 kHz, driver: 311-149887) for fast X-axis and a galvanometer scanner (8320K, driver: MicroMax 671) for slow Y-axis (both from Cambridge Technology, USA),
 - c. a general scan lens (LSM05-BB, Thorlabs, USA) with an effective focal length (EFL) of 110 mm,
 - d. a dedicated tube lens was custom designed combining three plano-convex lenses (Edmund Optics: 86-925), each with clear aperture and EFL of 73.5 mm and 500 mm, respectively, resulting in a combined EFL of 166.7 mm,
 - e. a high-NA and low magnification objective lens (Olympus XLUMPlanFI, 20 \times /0.95W) with an EFL of 9 mm.
9. Optically couple pulsed laser output to the resonant scanning mirror. Note that prior to coupling, the laser output must be sufficiently expanded to fulfill the clear aperture of the resonant scanning mirror. Depending on the laser beam diameter, a suitable beam expander can be chosen.
10. Optically couple the resonant scanning mirror to the galvanometer scanning mirror as depicted in [Figure 1](#). Note that one must try to minimize the distance between these two mirrors. We recommend \sim 12.5 mm separation between the centers of CRS 4 kHz and 8320K scanning mirrors.
11. Optically couple the galvanometer scanning mirror to LSM05-BB. The recommended separation between the galvanometer mirror and the front surface of LSM05-BB is 66 mm.
12. Optically couple LSM05-BB to the custom tube lens unit. The recommended separation between the last surface of LSM05-BB to the front surface of the custom tube lens is 261 mm.

- a. Build the custom tube lens by means of combining three plano-convex lenses (Edmund Optics: 86-925). The separation between each lens is recommended to be close to zero. A minor separation can be maintained to prevent surface damage. As depicted in [Figure 1](#), we recommend the flat surface to point toward the objective side.
 - b. For mounting the lenses, three adjustable ring mounts, such as, 03-670, Edmund Optics, can be used. The three mounts should be placed in series with minimal separation and are expected to be parallel to each other. The height of the three mounts should be maintained the same.
 - c. Note that a large clear aperture helps extend the scanning angle.
 - d. Note that splitting of the optical power, in this case, helps reduce spherical aberration.
13. Optically couple the custom tube lens to XLUMPlanFI, 20x/0.95W. The separation between the last surface of the custom tube lens unit to the back aperture of the objective lens is recommended to be 172 mm.

Optional: As depicted in [Figure 1](#) schematics, we recommend 3 steering mirrors 1, 2, and 3, to provide a compact optical design. Note that the mirrors are expected to be large enough to incorporate the scanning beam. Therefore, at least a $50 \times 50 \text{ mm}^2$ mirror size is recommended. While choosing the same, surface flatness of at least one-fourth of the wavelength is expected. The position of the mirrors can be adjusted as per the design/experimental requirements. We further recommend using an appropriate Faraday Optical Isolator right behind the high-intensity laser output to avoid any back reflection into the laser cavity. This becomes critical especially when the laser is not equipped with an internal isolator.

Note: Following [Equation \(11\)](#), targeting a fast-axis FOV of up-to 1.6 mm, the LAORS system requires a fast-X-axis scanning angle of up-to $\sim \pm 7.7^\circ$ with respect to the optical axis. With a 9.25 mm input beam diameter, the root mean square (RMS) wavefront errors (without defocus) and Strehl Ratios were found to be $< 0.07\lambda$ and $> 80\%$, respectively, for 0° and $\pm 7.7^\circ$ off-axis configurations along the fast X and slow Y axes, being optimized at a wavelength $\lambda = 1,070 \text{ nm}$ (presuming a typical Yb-fiber laser) while considering the objective lens to be a perfect one. [Figures 2A–2C](#) depict modulus of the optical transfer function (OTF) versus spatial frequency (cycles/mm) for angles of $\pm 7.7^\circ$ off-axis in the X direction, 0° off-axis in X and Y directions, and $\pm 7.7^\circ$ off-axis in the Y direction, respectively.

Note: The recommended optical design parameters, such as a separation between two surfaces, are based on Zemax simulation and are applicable only with our specified optical components. If you opt for relevant alternatives (especially the lenses), a simulation might be essential to optimize the parameters.

Note: Following [Equation 12](#) for our specific system configuration, we obtain a minimum required laser repetition rate of 60 MHz. Therefore, we opted for Fidelity 2 laser (Coherent, USA) with a 70 MHz repetition rate, a 1,070 nm central wavelength, and a < 60 femtosecond pulse width. Note that considering [Equation 5](#), we are now restricted to employing a synchronized sampling with $N = 1$, i.e., one-pulse-per-voxel. Following [Equation 9](#), NFOM thus turns out to be greater than one, i.e., the digitization becomes guaranteed to be aliasing-free.

Construction of the fluorescence collecting optics for the LAORS system

⌚ Timing: 1 day

14. [Figure 3](#) illustrates a schematic of fluorescence collecting optics, an essential part of the LAORS system, comprising:
 - a. a primary dichroic beam-splitter (FF801-Di02 or FF735-Di02, Semrock),
 - b. a relay system made up of two lenses with EFLs of 150 mm (Edmund Optics: 32-982) and 40 mm (Edmund Optics: 48-654), respectively,

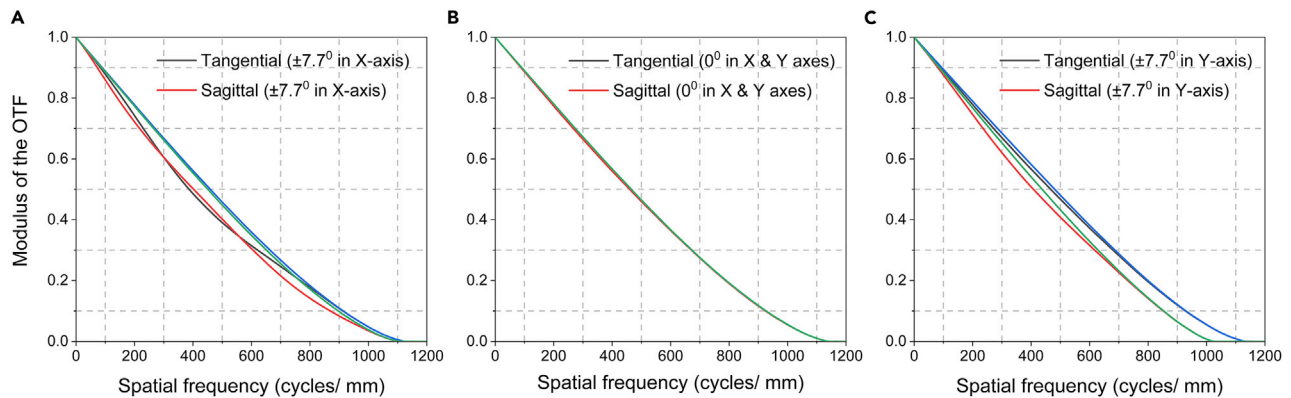


Figure 2. Modulus of the optical transfer function (OTF) vs spatial frequency (cycles/mm)

(A–C) Modulus of the OTF obtained for angles (over the scan lens) of (A) $\pm 7.7^\circ$ off-axis in X direction, (B) 0° off-axis in X and Y directions, and (C) $\pm 7.7^\circ$ off-axis in Y direction; optimized at a wavelength of 1,070 nm. Note: data obtained from Zemax; blue and green curves in each plot represent the diffraction limit curves for the tangential and sagittal cases, respectively.

- c. a photomultiplier tube (PMT, R10699, Hamamatsu Photonics, Japan),
- d. one or more relevant bandpass filter(s), such as FF01-580/60-25-D, Semrock.
15. Place the dichroic beam splitter prior to the back-aperture of the objective lens which will help reflect the emerging fluorescence signal towards the photosensitive area of the PMT.
16. For efficiently focusing the fluorescence signal, make use of a relay system as illustrated in [Figure 3](#). With a demagnification factor of 3.75, a ~ 4 mm focused spot diameter is ensured throughout the scanning range. Note that R10699 provides a 24×8 mm² photosensitive area which is large enough to support the 4 mm-wide focused spot.
17. Place appropriate band pass filter(s) prior to the photosensitive area of the PMT to ensure detection of the specific signal of interest. For instance,
 - a. Use FF01-580/60-25-D, Semrock to ensure detection of Nav1.8-tdTomato or Alexa Fluor 546 two-photon fluorescence signals.
 - b. Use an additional color glass filter in series (FGB37-A, Thorlabs) to reject any residual reflection of the excitation wavelength.

Construction of the control and data acquisition system

⌚ Timing: 5–7 days

18. Prepare the computer. The requirements are enlisted in [Table 1](#). A simple block diagram representation of the control and data acquisition system is depicted in [Figure 4](#).
 - a. Make sure the computer is powered off.
 - b. Install the cards at appropriate PCIe slots (recommended: PCIe 3.0 standard).
 - i. Place Quadro RTX 8000 or another alternative CUDA-enabled graphics card in an $\times 16$ slot.
 - ii. Place ATS9440 or another alternative AlazarTech digitizer in an $\times 8$ or higher bandwidth slot.
 - iii. Place PCIe-6341 or another alternative National Instruments multifunction I/O card in an $\times 4$ or higher bandwidth slot.
19. Connect CRS 4 kHz and 8320K to the respective driver boards. Ensure a stable power supply for each driver.
20. Connect the laser pulse sync signal from Fidelity 2 to the external clock input of ATS9440.
21. Feed the electrical signal from R10699 to C6438-01 and connect the amplified output to the first analog input (channel A) of ATS9440.

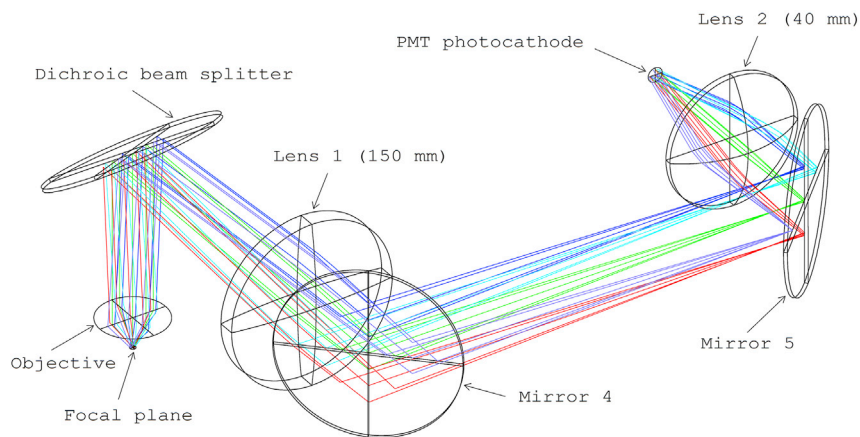


Figure 3. Schematics of the fluorescence collecting optics with Zemax ray tracing

The fluorescence collecting unit comprises of a primary dichroic beam splitter: FF801-Di02 or FF735-Di02, Semrock; a lens 1: Edmund Optics: 32-982, EFL of 150 mm, a lens 2: Edmund Optics: 48-654, EFL of 40 mm; a photomultiplier tube (PMT): R10699 (Hamamatsu Photonics, Japan). The turning mirrors are optional.

22. Feed the line trigger sync signal from CRS 4 kHz driver to a voltage buffer (50LD, Thorlabs), and by means of ZFRSC-42-S+, split the output into two: Sync-A and Sync-B.
 - a. Connect Sync-A to the external trigger input of ATS9440.
 - b. Connect Sync-B to PFI14 of PCIe-6341.
23. Connect the amplitude control pin of the CRS 4 kHz driver to the AO 0 pin of PCIe-6341.
24. Insert 6757 DAC to MicroMax 671 driver.
 - a. Plug the ribbon cable to 6757 DAC. Follow the indication on the cable to ensure which end should be plugged to the 6757 unit.
 - b. Connect the other end of the ribbon cable to PCIe-6341 digital I/O pins.
 - i. Make sure that DB0-DB15 pins of 6757 are connected to P0.0-P0.7 and P1.0-P1.7 pins of PCIe-6341 sequentially.
 - ii. Make sure that CLR, R/W, CS, and LDAC of 6757 are connected to P2.0-P2.3 pins of PCIe-6341 sequentially.
 - iii. Make sure that all ground pins of 6757 are connected to the digital ground of PCIe-6341.
25. Connect TSDM40-15X and SGSP80-20ZF units (or other alternatives from Sigma Koki) to SHOT-304GS.
 - a. SGSP80-20ZF is dedicated to sample displacement along the axial direction.
 - b. Two units of TSDM40-15X are dedicated to sample displacement along the horizontal and vertical directions.
 - c. Note that the TSDM40-15X units are to be attached in a way that their axes of motion are perpendicular to each other and this combined unit should be connected to the moving plate of the SGSP80-20ZF unit.
 - d. For holding a sample specimen, we recommend use of a typical sample holder, such as MPSH or MPSHSS, Thorlabs.
26. Connect R10699 to C9525 (make sure a good-quality HSV cable is used).
27. Connect SHOT-304GS and C9525 to the computer through USB cables.
28. Connect the output of R10699 to C6438-01 and feed the amplified output of C6438-01 to Channel A of ATS9440.

Optional: 50LD or other alternative is required only if the line trigger signal from CRS driver is with high impedance, and the relevant digitizer/interface card input is with low impedance. A phase matching circuit can be employed optionally to fine-tune sampling events with the laser-pulses to best optimize signal collection.

Control & Data Acquisition System

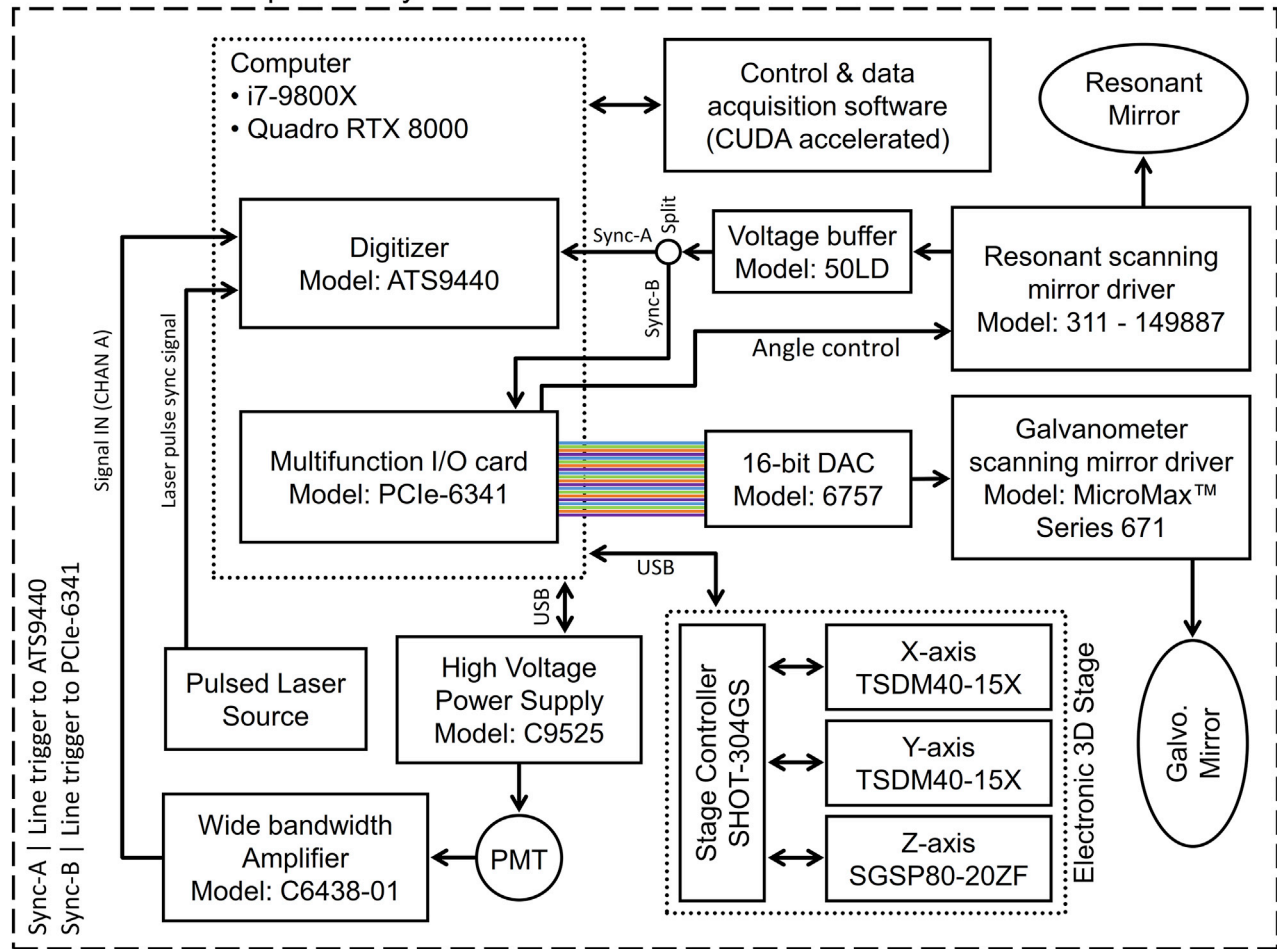


Figure 4. Block diagram of the proposed control and data acquisition system

The system comprises of- a computer: with i7-9800X 8-core processor and Nvidia Quadro RTX 8000 for CUDA-acceleration; a multifunction I/O card: PCIe-6341 (National Instruments Corporation, USA); a digitizer: ATS9440 (Alazar Technologies Inc., Canada); a 70 MHz pulsed laser source: Fidelity 2 Yb-Fiber Laser (Coherent Inc., USA); a resonant scanning system: CRS 4 kHz (driver: 311-149887), a galvanometer scanning system: 8320K (driver: MicroMax 671), Cambridge Technology, USA; a 16-bit digital to analog converter (DAC): 6757 (Cambridge Technology, USA); a voltage buffer: 50LD (Thorlabs, USA); a power splitter: ZFRSC-42-S+ (Mini-Circuits, USA); a high voltage power supply: C9525 (Hamamatsu Photonics, Japan); a transimpedance amplifier: C6438-01 (Hamamatsu Photonics, Japan); a multi-axis stage controller: SHOT-304GS, and three linear stages: 2 × TSDM40-15X and 1 × SGSP80-20ZF (Sigma Koki, Japan); a software: C++ written custom application.

Note: C6438-01 receives output from PMT R10699 and produces an amplified signal. ATS9440 uses the laser pulse sync signal as external clock input and triggers the sampling events. Our custom software handles slow-axis-synchronization, data acquisition, preview, and export processes. We enable synchronization of slow Y-axis with fast X-axis without sending an external electrical frame-trigger signal after completion of each frame. A background high-priority thread monitors the line trigger events from the resonant scanning mirror driver and produces 16-bit binary data words (generating a sawtooth waveform), i.e., the slow-axis angle-positioning-steps to 6757 DAC.

Installing LASERaster⁺

⌚ Timing: <45 min

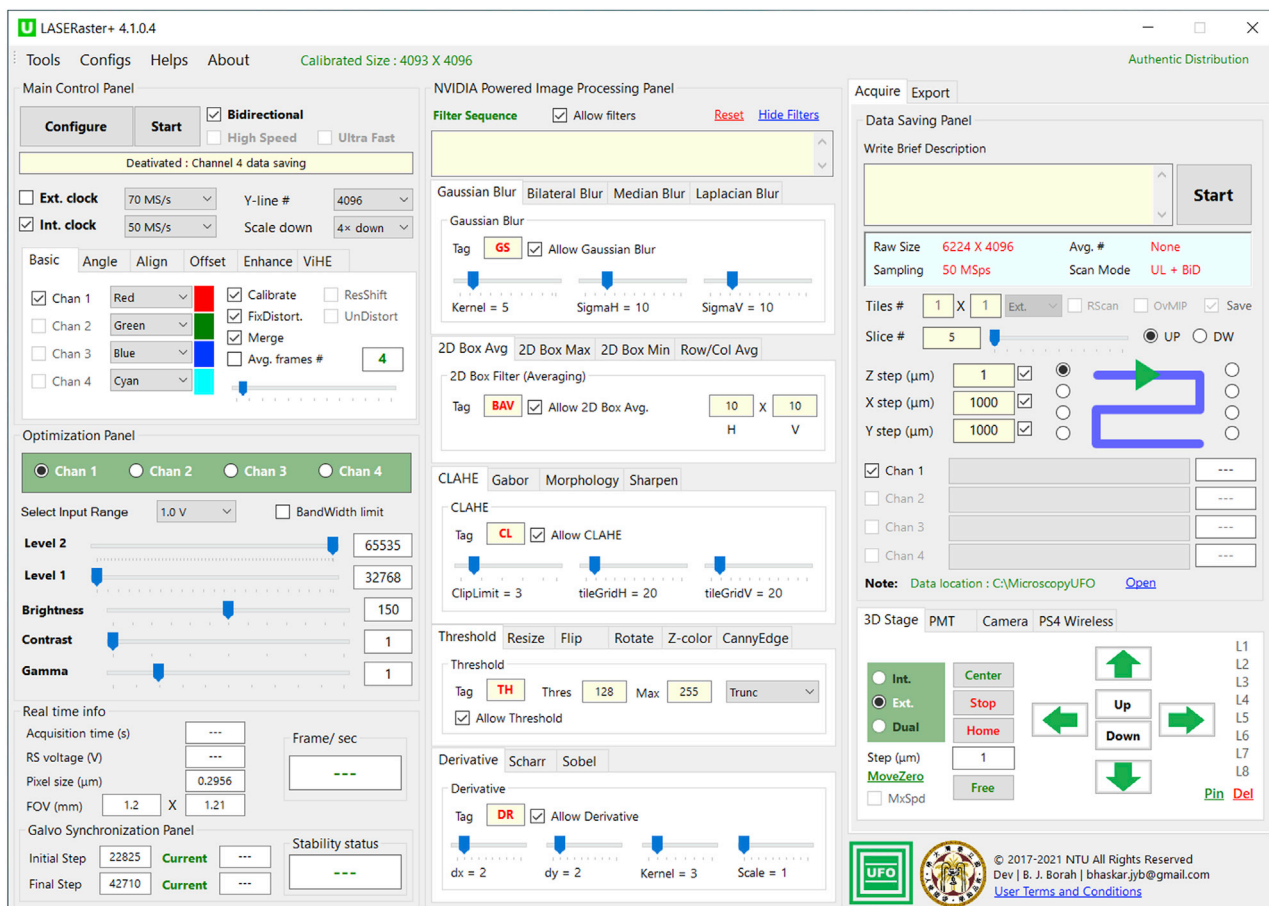


Figure 5. Graphical user interface of LASERaster⁺

The compiled standalone version with enabled stable features with relevant operational manual would be available from [lead contact](#).

Follow the below steps carefully to install the software.

29. Obtain the *SetUp LASERaster⁺.exe* file from the [lead contact](#).
30. Run *SetUp LASERaster⁺.exe*.
 - a. If prerequisite(s) is/are not found, installer will redirect to relevant site(s) to help download the specific driver(s)/software.
 - i. Prerequisite 1: .NET framework (4.6.1 or newer).
 - ii. Prerequisite 2: NVIDIA driver (30.0.0 or newer).
 - iii. Prerequisite 3: Alazar card driver (6.7.0 or newer).
 - iv. Prerequisite 4: NIDAQmx runtime (18.6.0 or newer).
 - b. Note that if the NI-DAQmx is newer than 18.6, install the NI package manager first, and make sure to only check "NI-DAQmx Support for C" during the installation process.
 - c. Note that software installation will proceed only after the above requirements are fulfilled.
31. After successful installation, run *LASERaster⁺* and follow the instructions to activate the software. [Figure 5](#) shows the graphical user interface of *LASERaster⁺*.

Note: *LASERaster⁺* uses a multithreaded slow-axis synchronization algorithm, without the need for an external frame-trigger signal. A high priority background thread monitors line trigger (Sync-B) signal, and accordingly produces 16-bit data words, i.e., angle-positioning steps (generating a sawtooth waveform) to 6757 DAC unit, all by means of PCIe-6341 interfaced to the computer motherboard.

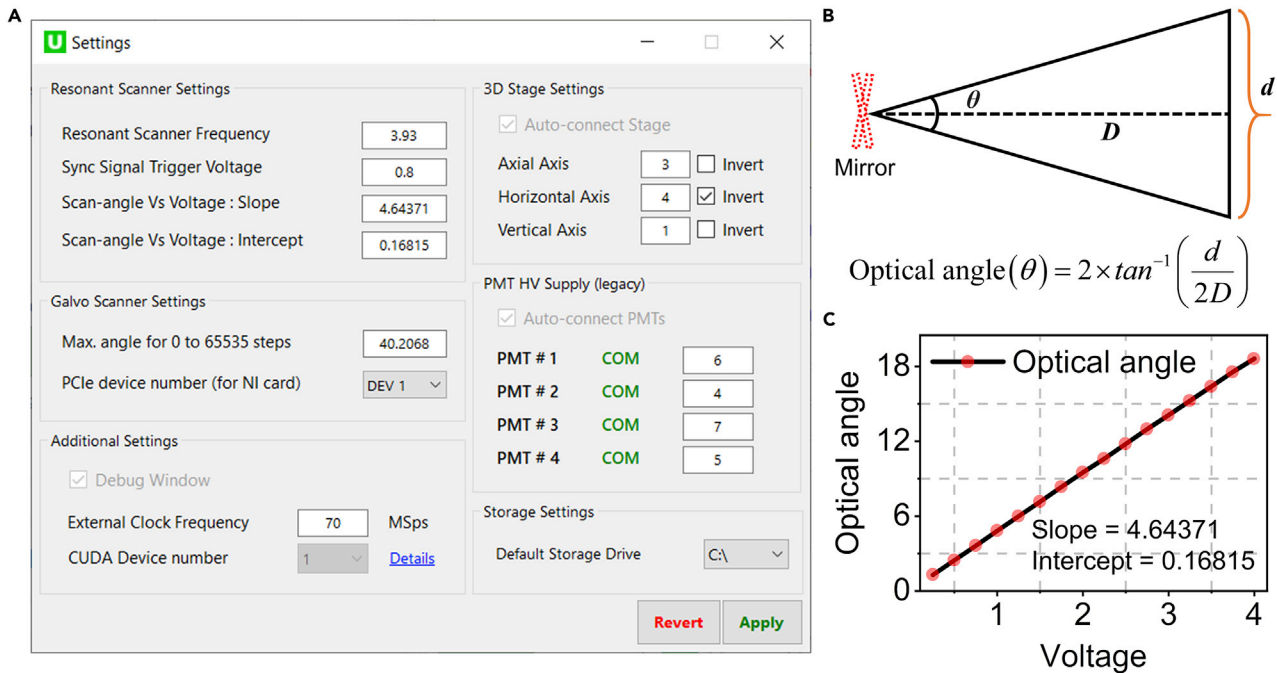


Figure 6. Entering a few important settings prior to imaging

(A) The Settings GUI with multiple panels for resonant & galvanometer scanners, 3D stage, PMT high voltage (HV) supply, and additional parameters. (B and C) Calibration of resonant scanning angle, where B shows a simple method to estimate a scanning angle (optical) and C depicts a linear fitted plot for voltage vs optical scanning angle.

Set a few important parameters

⌚ Timing: 2 h

32. Click *Tools* and then *Settings*. The panel depicted in [Figure 6A](#) will appear.
33. Enter Resonant Scanner Settings.
 - a. *Resonant Scanner Frequency*: measure the actual frequency of your resonant scanner using an oscilloscope and enter the value in kHz unit.
 - b. *Sync Signal Trigger Voltage*: keep the default value.
 - c. *Scan-angle Vs Voltage: Slope & Intercept*: to obtain the same, a simple experiment is required. Align a visible laser to the resonating mirror and let the reflected beam fall on a wall. The optical angle (θ) can be obtained as shown in [Figure 6B](#), following $\theta = 2 \tan^{-1}(0.5d/D)$.
 - i. Enable *Alignment mode* [Refer to *Main Control Panel* → *Align*].
 - ii. Gradually increase *RS-angle*. For each step, note down the *RS voltage (V)* [to amplitude control pin, CRS driver] depicted in *Real time info* panel, and then calculate θ .
 - iii. Plot voltage vs optical angle as shown in [Figure 6C](#). Enter the linear-fitted slope and intercept.
 - iv. Note that this voltage is applied to the amplitude control pin of the CRS 4 kHz driver connected to the AO 0 pin of PCIe-6341.
34. Enter Galvo Scanner Settings.
 - a. *Max. angle for 0 to 65,535 steps*: align the visible laser to the galvanometer mirror and let the reflected beam fall on a wall. In *Alignment mode* set *Galvo step* to 0 and mark the laser spot position. Similarly, mark a second position for the 65535th step. Calculate the angle and enter the same.
 - b. *PCIe device number (for NI card)*: change it to DEV 2, DEV 3, or other, only if the software is not able to control the scanners. Note that this step is recommended if steps 33.c (i–iii) fail.

35. Enter Additional Settings.
 - a. *External Clock Frequency*: enter your laser repetition rate in MHz unit (MSps denotes mega samples per second). Make sure to confirm the exact value with an oscilloscope.
36. Under *3D Stage Settings*, enter axis numbers (refer to your SHOT-304GS unit) for your axial, horizontal, and vertical linear stages. If you require a stage to move in the opposite direction, check the respective *Invert* option. Note that there is no need to specify the COM port, as the software will auto-detect the same.
37. Under *PMT HV Supply*, specify the COM port of your C9525 unit.
38. Under *Storage Settings*, feel free to change your *Default Storage Drive*. Make sure the drive is with a fast enough read/write capability [recommended: PCIe SSD].
39. Click *Apply* to save the settings.

Optional: To get *Max. angle for 0 to 65,535 steps*, you can alternatively follow the maximum angle specified by the manufacturer.

Try scanning and exporting data

⌚ Timing: 10 min

40. Referring to *Main Control Panel*, Click *Configure* and then *Start*.
41. To start saving data, refer to *Data Saving Panel* and *Start*. Note that 16-bit data will be saved in binary format.
42. To load and export an existing data set, refer to *Data Read Panel*.
 - a. Check *Activate Viewer*.
 - b. Click *Load*, then navigate and select your data location.
43. To export the data, refer to *Batch Export Settings*.
 - a. Select frames to export.
 - b. Click *Export* and select a destination directory.

Note: Refer to *Data Saving Panel* to set *Slice #*, *Z step (μm)*, and axial motion direction (*UP/DW*) while acquiring an imaging stack at a specific lateral (*XY*) position.

Basic calibration of FOV

⌚ Timing: 3 h

For FOV calibration, you need to image a standard test target along both horizontal and vertical directions. We recommend a 1 mm stage micrometer (R1L3S2P, Thorlabs). In our demonstration, R1L3S2P was imaged via third-harmonic generation (THG) signal. Ensure a low average excitation power to reduce damage to the target.

44. Click *Tools* and then *Calibrations*. The panel depicted in [Figure 7A](#) will appear.
45. Enter the following straightforward acquisition parameters:
 - a. *RS Freq (kHz)*: resonant scanner frequency in kHz.
 - b. *Sampling (MSps)*: sampling rate in mega samples per second.
 - c. *Resonant Scanner Angle (Optical Angle)*: fast axis scanning angle in degrees.
 - d. *Y-line #*: number of lines scanned along slow Y-axis.
 - e. *Y-steps/ Line*: number of steps specified for each line.
46. To estimate *Y-FOV (mm)*, export the vertical image of the stage micrometer as depicted in [Figure 7B](#), and accordingly calculate and input the Y-FOV in millimeter.
47. Note that estimation of *X-FOV (mm)* is not quite straightforward, because resonant scanner induces a nonlinear distortion due to its cosinusoidal motion. Distortions must be corrected prior to estimating X-FOV.

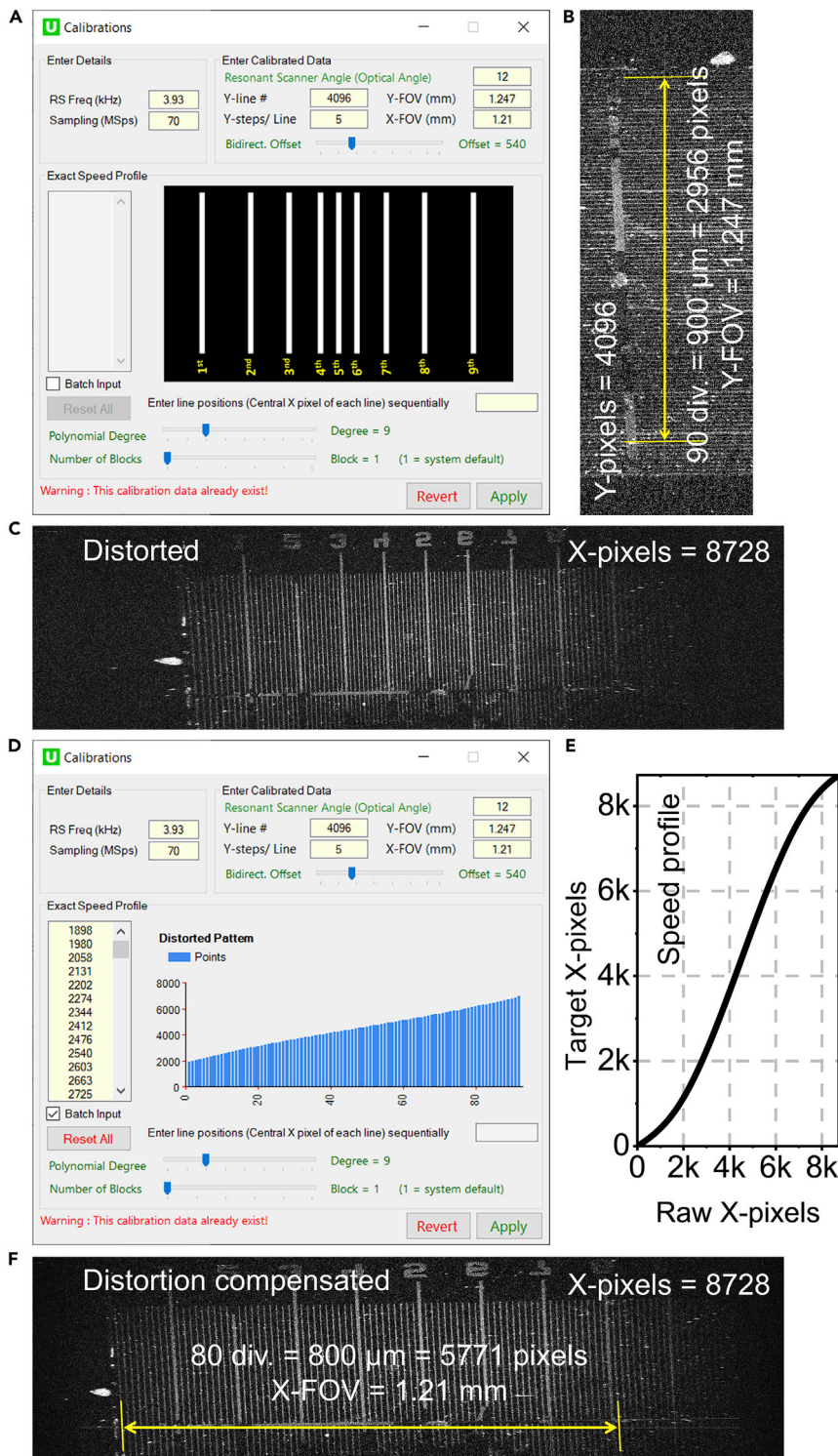


Figure 7. Basic calibration of FOV

(A) The Calibrations GUI.

(B) Vertical image of stage micrometer; Y-pixel number = 4096, estimated Y-FOV = 1.247 mm.

(C–E) (C) Horizontal image of stage micrometer with no distortion compensation; (D) entering X-pixel coordinates of the lines in C; (E) plot of an estimated speed profile.

(F) Distortion compensated horizontal image of stage micrometer; X-pixel number = 8728, estimated X-FOV = 1.21 mm.

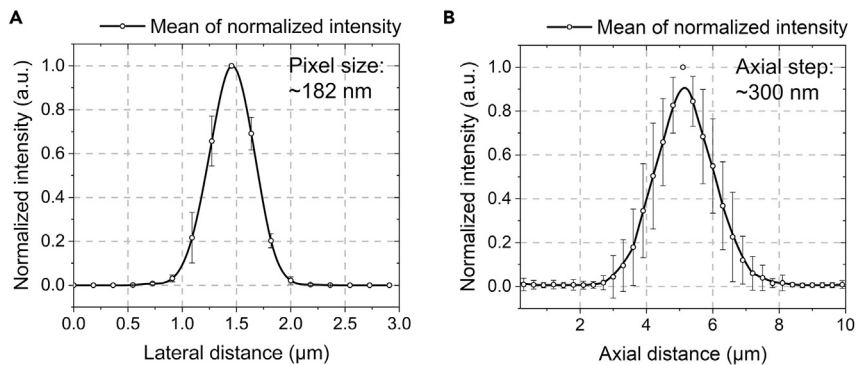


Figure 8. Two-photon resolution analysis using fluoresbrite microspheres

(A and B) (A) Lateral, and (B) axial cross-sections; averaged data considering 25 microspheres from the central-FOV; error bars denote standard deviations. Lateral and axial resolutions are found to be around $0.483 \pm 0.034 \mu\text{m}$ and $1.997 \pm 0.303 \mu\text{m}$, respectively. No optical zooming was employed.

- a. Typically, we can assume that distortion in a digitized image is symmetric in nature. In that case, there is no need to enter any detail in *Exact Speed Profile* panel, and directly proceed to the next step.
- b. It is possible that there exists a phase mismatch between the mechanical edge of the resonating mirror and starting of each fast-axis line leading to an asymmetric distortion, which might require a hardware-based calibration. In such a case, we offer the following steps to obtain the exact speed profile:
 - i. Export horizontal image of the stage micrometer (as depicted in [Figure 7C](#)) with disabled *Calibrate Images* and *Fix Distortion* in *Batch Export Panel*.
 - ii. As shown in [Figure 7D](#), sequentially enter the X-pixel coordinate of each vertical line in [Figure 7C](#). Check *Batch Input* to paste all values at once. Make sure to include lines from both left and right halves of the image (not necessarily from extreme edges). Keep *Polynomial Degree* and *Number of Blocks* at default values. Note that based on the distribution of lines, the complete speed profile would be estimated as plotted in [Figure 7E](#).
 - iii. Enter a roughly estimated X-FOV value for now and click *Apply*.
48. Export horizontal image of stage micrometer as depicted in [Figure 7F](#), with disabled *Calibrate Images* but enabled *Fix Distortion*, and accordingly calculate and enter the X-FOV in millimeters.
49. Click *Apply* to save the calibrations.

Note: we follow the idea by [Haji-Saeed et al. \(2007\)](#) to correct nonlinear distortion along the fast X-axis. The algorithm was implemented via CUDA-acceleration for real-time applicability.

EXPECTED OUTCOMES

To validate the high-NFOM nature of the constructed MPM, we performed a two-photon resolution analysis as depicted in [Figure 8](#). Fluoresbrite microspheres (Catalog No. 24050-5, Polysciences, Inc., diameter of 200 nm) were first immobilized by immersing in a 0.7% agarose solution, and subsequently, two-photon imaging was performed at a central excitation wavelength of 1,070 nm while maintaining a large 1.6 mm-wide FOV. [Figures 8A](#) and [8B](#) plot lateral and axial cross-sections considering measurements from 25 microspheres. Note that error bars denote standard deviations. By means of Gaussian fitting, effective lateral and axial resolutions were found to be around $0.483 \pm 0.034 \mu\text{m}$ and $1.997 \pm 0.303 \mu\text{m}$, respectively. We further evaluated the two-photon resolution towards the edges of the FOV considering averaged data from 6 beads, and the lateral and axial resolutions were found to be around $0.49 \pm 0.03 \mu\text{m}$ and $3.31 \pm 0.26 \mu\text{m}$, respectively. Note that with a

pixel size of 182 nm, no optical zooming was required in this analysis while retrieving a 0.48 μm digital resolution being comparable to our objective limited resolution of $\sim 0.43 \mu\text{m}$.

LIMITATIONS

An objective lens with a limited field number induces vignetting effect towards the corners of a square shaped FOV especially at larger scanning angles. To enable uniform and artifact-free mosaic-stitching, the FOV is thus recommended to be lowered so as to reduce vignetting. Note that an adaptive optics system and/or custom manufactured optical components together with a high field number objective lens can help minimize this issue. Besides various digital image processing methods, such as, but not limited to, contrast limited adaptive histogram equalization (CLAHE) (Reza, 2004) can be used to improve reduced off-axis signal strength. A maximized square-shaped FOV might not be suitable for a high frame-rate functional analysis. We recommend lowering the slow-axis pixel number, and hence the slow-axis FOV to boost the imaging frame rate for such an application.

TROUBLESHOOTING

Problem 1

Error messages (in red color) might appear in *3D Stage* and *PMT* panels while trying to access/control the relevant devices.

Potential solution

- Make sure that C9525 and SHOT-304GS (or other alternatives) are properly connected to the computer each with a good quality USB cable.
- Restart your computer.
- Go to Device Manager and check under Ports (COM & LPT) to make sure the relevant devices are detected by Windows.
- Launch the software and check if the error messages are gone.
- In the case of C9525, make sure to note its COM port and enter the same in the *PMT HV Supply* panel. Note that after applying a change, the software will relaunch.
- If the issue is not solved yet, power off C9525 and/or SHOT-304GS, wait for a few seconds and turn that on again. Relaunch the software.

Problem 2

While starting an acquisition with *Ext. Clock* enabled, the software might show *Error: AlazarWait AsyncBufferComplete Failed*.

Potential solution

This error indicates that the laser-pulse sync signal is not detected. Make sure the laser is on and its sync output is properly connected to the Alazar digitizer.

Problem 3

While starting an acquisition, the software might show *Error: No Trigger Detected*.

Potential solution

This error indicates that we could not detect the line trigger signal from CRS driver. Make sure 50LD is properly powered with a USB cable. Disconnect and reconnect the input signal to 50LD. If the issue is not yet solved, power off the computer and CRS scanner, wait for a few seconds and power them on again.

Problem 4

Due to electromagnetic interference (EMI), you might see artifacts in a contrast-enhanced image, especially when the image does not consist of any bright structures.

Potential solution

We strongly recommend adequately covering a PMT socket with EMI shielding foil to minimize such artifacts.

RESOURCE AVAILABILITY

Lead contact

Further information and requests for resources should be directed to and will be fulfilled by the lead contact, Chi-Kuang Sun (sun@ntu.edu.tw).

Materials availability

This study did not generate new unique reagents.

Data and code availability

The data/images generated and/or analyzed to support our findings are presented in this protocol. More details are available from the [lead contact](#) upon reasonable request. This protocol does not report the original code.

ACKNOWLEDGMENTS

This project was supported by the Ministry of Science and Technology (Taiwan) with financial grant MOST 111-2321-B-002-015- and Ministry of Economic Affairs (Taiwan) with financial grant 111-EC-17-A-19-S6-009. We thank Dr. Daniel Lin (SunJin Lab Co., Taiwan), Dr. Jye-Chang Lee, and Prof. Chen-Tung Yen (Department of Life Science, National Taiwan University, Taipei 10617, Taiwan) for advice and support in biological sample preparation.

AUTHOR CONTRIBUTIONS

B.J.B. designed, optimized, and implemented the reported protocol(s); developed the C++-based control and data acquisition software; and performed imaging experiments and relevant data analysis. C.-K.S. initiated the concept and conducted the research. B.J.B. and C.-K.S. wrote the protocol.

DECLARATION OF INTERESTS

The reported opto-electro-mechanical design aspects are under national-phase patent applications through the Patent Cooperation Treaty (PCT), publication number: WO/2021/112942; approved USA and Taiwan patents; inventors: C.-K. Sun & B.J. Borah; applicant: National Taiwan University, Taiwan. The free version of the acquisition software is available from the corresponding author upon reasonable request, for non-commercial use only, subject to regulations of National Taiwan University, Taiwan.

REFERENCES

- Borah, B.J., Lee, J.-C., Chi, H.-H., Hsiao, Y.-T., Yen, C.-T., and Sun, C.-K. (2021). Nyquist-exceeding high voxel rate acquisition in mesoscopic multiphoton microscopy for full-field submicron resolution resolvability. *iScience* 24, 103041.
- Bumstead, J.R., Park, J.J., Rosen, I.A., Kraft, A.W., Wright, P.W., Reisman, M.D., Côté, D.C., and Culver, J.P. (2018). Designing a large field-of-view two-photon microscope using optical invariant analysis. *Neurophoton.* 5, 025001.
- Chun, W., Do, D., and Gweon, D.G. (2013). Design and demonstration of multimodal optical scanning microscopy for confocal and two-photon imaging. *Rev. Sci. Instr.* 84, 013701.
- Denk, W., Strickler, J.H., and Webb, W.W. (1990). Two-photon laser scanning fluorescence microscopy. *Science* 248, 73–76.
- Haji-Saeed, B., Khoury, J., Woods, C.L., Pyburn, D., Sengupta, S.K., and Kierstead, J. (2007). Mapping approach for image correction and processing for bidirectional resonant scanners. *Opt. Eng.* 46, 027007.
- Heintzmann, R., and Sheppard, C.J.R. (2007). The sampling limit in fluorescence microscopy. *Micron* 38, 145–149.
- Li, R., Wang, X., Zhou, Y., Zong, H., Chen, M., and Sun, M. (2018). Advances in nonlinear optical microscopy for biophotonics. *J. Nanophoton.* 12, 033007.
- Nyquist, H. (1928). Certain topics in telegraph transmission theory. *Trans. AIEE* 47, 617–644.
- Pawley, J.B. (2006). Points, Pixels, and Gray Levels: Digitizing Image Data. In *Handbook of Biological Confocal Microscopy*, J.B. Pawley, ed. (Springer), pp. 59–79.
- Reza, A.M. (2004). Realization of the Contrast Limited Adaptive Histogram Equalization (CLAHE) for Real-Time Image Enhancement. *The Journal of VLSI Signal Processing-Systems for Signal, Image, and Video Technology* 38, 35–44.
- Shannon, C.E. (1949). Communications in the presence of noise. *Proc. IRE* 37, 10–21.
- Sheppard, C., and Gu, M. (1990). Image formation in two-photon fluorescence microscopy. *Optik* 86, 104–106.
- Sofroniew, N.J., Flickinger, D., King, J., and Svoboda, K. (2016). A large field of view two-photon mesoscope with subcellular resolution for in vivo imaging. *eLife* 5, e14472.

Stirman, J.N., Smith, I.T., Kudenov, M.W., and Smith, S.L. (2016). Wide field-of-view, multi-region, two-photon imaging of neuronal activity in the mammalian brain. *Nat. Biotechnol.* *34*, 857–862.

Terada, S.I., Kobayashi, K., Ohkura, M., Nakai, J., and Matsuzaki, M. (2018). Super-wide-field two-photon imaging with a micro-optical device moving in post-objective space. *Nat. Commun.* *9*, 3550.

Tsai, P.S., Mateo, C., Field, J.J., Schaffer, C.B., Anderson, M.E., and Kleinfeld, D. (2015). Ultra-large field-of-view two-photon microscopy. *Opt. Express* *23*, 13833–13847.

Yue, S., Slipchenko, M.N., and Cheng, J.-X. (2011). Multimodal nonlinear optical microscopy. *Laser Photon. Rev.* *5*, 496–512.

Zhang, Z., de Munck, J.C., Verburg, N., Rozemuller, A.J., Vreuls, W., Cakmak, P., van Huizen, L.M.G.,

Idema, S., Aronica, E., de Witt Hamer, P.C., et al. (2019). Quantitative third harmonic generation microscopy for assessment of glioma in human brain tissue. *Adv. Sci.* *6*, 1900163.

Zipfel, W.R., Williams, R.M., and Webb, W.W. (2003). Nonlinear magic: multiphoton microscopy in the biosciences. *Nat. Biotechnol.* *21*, 1369–1377.